6.78 MHz self-oscillating parallel resonant converter based on GaN technology

Conference Paper · March 2017

DOI: 10.1109/APEC.2017.7930912

CITATIONS
10

READS
532

4 authors:

Ricardo Bonache-Samaniego
Universitat Rovira i Virgili
5 PUBLICATIONS **50** CITATIONS
SEE PROFILE

Carlos Olalla
Universitat Rovira i Virgili
59 PUBLICATIONS **1,845** CITATIONS
SEE PROFILE

L. Martinez-Salamero
Universitat Rovira i Virgili
282 PUBLICATIONS **5,544** CITATIONS
SEE PROFILE

Dragan Maksimovic
University of Colorado Boulder
490 PUBLICATIONS **25,917** CITATIONS
SEE PROFILE

6.78 MHz Self-Oscillating Parallel Resonant Converter Based on GaN Technology

Ricardo Bonache-Samaniego, Carlos Olalla*
and Luis Martínez-Salamero
Industrial Electronics and Automatic Control Group
Universitat Rovira i Virgili, DEEEA Dept.
Campus Sescelades, Tarragona, Spain 43007
*carlos.olalla@urv.cat

Dragan Maksimović
Colorado Power Electronics Center
University of Colorado Boulder, ECEE Dept
425 UCB, Boulder, CO 80309-0425
maksimov@colorado.edu

***Abstract*—This paper describes the design of a 6.78 MHz self-oscillating parallel resonant power converter for wireless power transfer applications. By sensing just the polarity of the tank inductor current to generate the switch control signals, the system is able to auto-start and self-oscillate at the desired frequency only by applying power to the input port. Different current sensing techniques, including a current sensing transformer and a series resistor followed by a high-speed differential amplifier, are compared based on bandwidth limitations and noise rejection considerations. Furthermore, delay-compensation networks are included in order to mitigate effects of the propagation delays added by signal processing components in the feedback path. It is shown that the circuit is capable of meeting the A4WP/AirFuel standard specifications for wireless power charging. Both inverter and inverter+rectifier configurations are tested and their performances are verified by simulations and experiments on a 16 W prototype using GaN power devices, showing an efficiency of 98 % and 83 %, respectively.**

***Keywords*—Resonant Power Conversion, Parallel Resonant Converter, Self-Oscillating Control, Variable Structure System, High-frequency systems, Wireless Power Transfer, Alliance for Wireless Power, AirFuel Alliance, GaN.**

I. Introduction

Resonant converters represent the core of high-frequency wireless power transfer (WPT) systems, which offer easy-to-use single and multi-device charging for smartphones, tablets or small laptops [1], [2]. This work focuses on the development of a 6.78 MHz resonant power converter following the AirFuel Alliance transmitter standard [3]. This application area has been gaining attention and various solution approaches have been addressed in a number of papers [2]–[11]. Challenges include maintaining soft switching and optimum power transfer in the presence of variations in coupling, the resonant tank, and the power level.

With the objectives of switching near the resonant frequency (for optimum power transfer and reduced losses) and also of reducing the system complexity and cost, this paper explores a self-oscillating power converter to meet the application objectives. This new approach enables efficient power transfer for variable loads and resonant tanks [12]. However, the self-oscillation technique presents implementation challenges at high frequency, since propagation delays and parasitic effects play significant roles in the control signal stages. This work covers possible solutions to counteract these undesired effects and select the approach suitable for wireless power transfer applications in compliance with the class 3 AirFuel Alliance specifications.

The research leading to these results has received funding from: (i) the People Programme (Marie Curie Actions) of the European Union's Seventh Framework Programme (FP7/2007-2013) under REA grant agreement nř 626117, (ii) from the Spanish Ministry of Economy and Competitiveness under grants DPI2012-31580/BES-2013-063288, EEBB-16-10687 and DPI2013-47293-R.

II. Self-Oscillating Resonant Converter

Figure 1 shows the schematic of the converter prototype: it is composed of a full-bridge resonant converter with a parallel resonant tank. The prototype can be configured as an inverter, such that the load is connected directly to the output of the resonant tank, or it can also be configured as an inverter+rectifier configuration to accomplish dc-dc conversion.

For load impedance matching in wireless power transfer, the resonant converter is typically driven at the resonant frequency by an external oscillator. However, the switching pattern can also be generated by sensing the polarity of the resonant tank inductor current, so that the fundamental harmonic of the input voltage v_s is in phase with the input current i_s and the tank input impedance is resistive [13]. Given that this is only possible at one switching frequency, the circuit oscillates naturally at its resonant frequency.

The AirFuel Alliance standard specifies an input voltage between 8 and 32 V and an output RMS voltage in the same range with a maximum power of 16 W [3]. The nominal switching frequency is equal to f_{sw} = 6.78 MHz, with a tolerance of ± 150 kHz. In the design presented here, an input voltage of 12 V and an output AC voltage of 30 V RMS (42 V peak) are assumed, for a maximum load R_L of 57 Ω. Following the design rules presented in [12], the resonant inductance L and the resonant capacitance C are equal to 486.5 nH and 1.13 nF, respectively.

The following two subsections briefly describe the design considerations related to current sensing and the full-bridge realization of the circuit using GaN devices.

A. Current Sensor Design

This application requires accurate current sensing, given that the generation of the switching pattern entirely depends on the sensed current waveform. The sensing stage requires

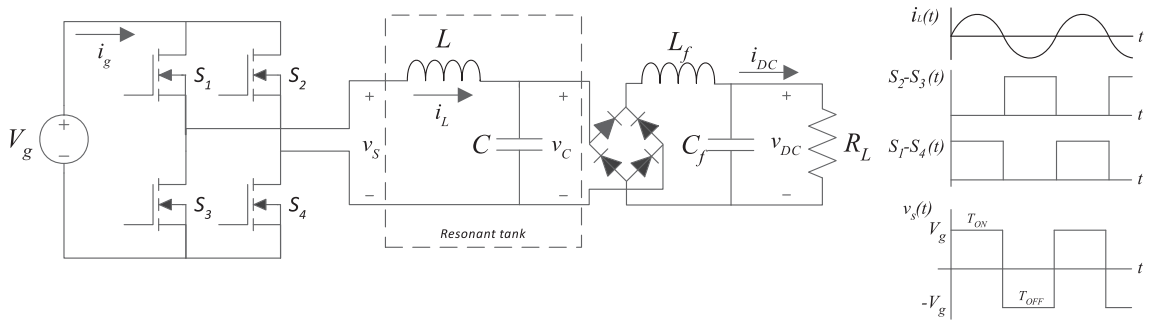

Figure 1. Circuit diagram of a resonant power converter (left) and switching-pattern signal generation waveforms (right).

Table I. COMPONENTS OF THE EXPERIMENTAL PROTOTYPE

Parameter	Code or Value
L (Design)	486.5 nH
C (Design)	1.13 nF
Differential Amplifier	THS4151
eGaN FET	EPC8004
Driver	LM5113

sufficiently large bandwidth, high-speed, and noise rejection in order to reproduce the current signal at 6.78 MHz. Moreover, parasitics can affect the response of the sensor and may require compensation. A classification of different sensing techniques, accounting for the fundamental frequency of the waveform, has been presented in [14, Table I]. Two main sensing techniques can be identified as suitable for high-frequency applications: (i) a current sensing transformer [15]–[17] or (ii) a series resistor sensed over a high-speed differential amplifier [14], [18], [19]. As presented in [16], [17] and [20], current sensing transformers require compensation of the parasitic effects generated between the windings by opposing the magnetic fields with a specific wiring design. In contrast, the shunt resistor sensor does not require any special procedure in order to operate at 6.78 MHz, and in consequence, this is the approach employed in this work. It is worth noting that the differential amplifier must exhibit appropriate gain, bandwidth and common-mode voltage rejection ratio. A high slew-rate THS4151 differential amplifier has been used in this case.

B. Full-Bridge Inverter Design

Due to the high switching frequency and the power level desired for the considered application, switches presenting low gate charge and reduced recovery times are preferred. Therefore, GaN FETs (EPC8004, $R_{\mathrm{DS_{(on)}}}$ = 110 mΩ, Q_{G} = 370 pC) have been used in this work, minimizing the parasitic effects that may impact the generation of the self-oscillating signal and the overall efficiency. Two LM5113 half-bridge drivers are used for the activation of the switches.

C. Summary of Selected Components

Table I summarizes the components of the current sensor and the power stage.

III. DELAY COMPENSATION NETWORK

One of the main limitations of the proposed self-oscillating approach is due to the adverse effects of propagation delays over the synchronization between the sign of the tank input current and the polarity of the tank input voltage. In the experimental prototype, the overall propagation delay is approximately 60 ns, which produces a mismatch with respect to the desired resistive input impedance and yields a significant reduction in the switching frequency. In conclusion, with practical components in the feedback path, a delay compensation network is required in order to eliminate these effects and meet the system requirements.

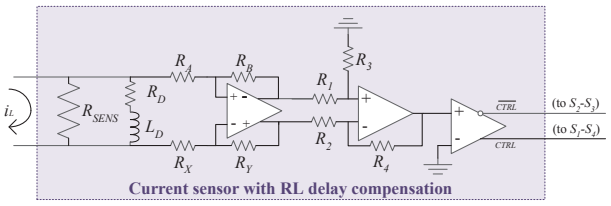

Figure 2. Phase-leading RL delay compensation network.

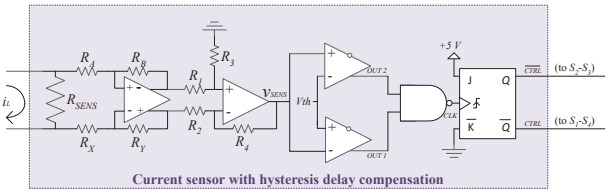

Figure 3. Hysteresis delay compensation network.

Two different compensation networks are considered:

- A phase-leading RL circuit inserted at the input of the current-sensing differential amplifier.
- An adjustable hysteresis applied to the input of the current polarity comparator.

A. Phase-Leading RL Compensation Network

This compensation network is based on an analog RL circuit that phase-shifts the voltage signal sensed by the shunt resistor R_{SENS}, as shown in Fig 2. Phase-shift can be adjusted by changing the value of R_D as defined by $\tau = \frac{L_D}{R_D}$, where τ is the value of delay to be compensated. The output of the sensor is then compared with zero so that the zero-crossings of the compensated waveform activate the corresponding switches.

Advantages of this solution are that it can process high bandwidth waveforms and that it remains invariable with

respect to load changes. However, this approach introduces losses and the compensation is sensitive to temperature variations and components tolerance. In addition, compensation can not be adjusted automatically, so the RL approach can be considered less practical compared to the hysteresis-based approach discussed next.

B. Hysteresis-Based Compensation Network

It is also possible to compensate the delay by changing the instant when the switching pattern is generated using an adjustable hysteresis function. This hysteresis allows the user to set a comparison value different than 0, enabling the system to switch at a defined time before the zero-crossing point of the current. As the system exhibits an approximately constant delay, compensation can be successfully achieved by setting a constant hysteresis value. In addition, the hysteresis value can be adjusted to obtain zero voltage switching (ZVS) operation while maintaining the switching frequency very close to the resonant frequency.

Fig. 3 depicts the block diagram of this compensation network. A rising-edge activated monostable is introduced in order to keep 50 % duty cycle, such that compensation is achieved equally during T_{on} and T_{off}. The comparators are in inverse configuration, such that there exists a period when both are activated, corresponding to the current sense signal within $+V_{th}$ and $-V_{th}$. The outputs of the comparators are later combined with a NAND or an AND gate, which establishes the clock switching pattern of the monostable. The AND gate can be employed in case of delays below one half of the on/off periods, whereas the NAND gate must be provided in case of delays between one half and the entire period. In the proposed prototype, every on/off period lasts 80 ns, so that the reported delay of 60 ns requires the NAND gate. Figure 4 illustrates the generation of the delay-compensated driving signal with the AND and the NAND gates. The range of operation of each logic gate is highlighted.

The proposed hysteresis-based circuit has several merits, including low latency, accuracy and the capability of compensating delays longer than half of the switching cycle. However, the circuit also presents some limitations. First, the hysteresis compensation may inhibit the auto-startup of the self-oscillation. The initial trajectory of the input current may not present sufficient amplitude to intersect $V_{th}/-V_{th}$ values, thus preventing the switching of the monostable and blocking the start-up of the power converter. The issue can be solved by introducing a startup-ramp behavior in the hysteresis level generator. The hysteresis is initially zero, and increases up to the desired steady-state value with a sufficiently gentle slope. In order to maintain a simple implementation, this behavior has been realized with a RC low-pass filter, as shown in Fig. 5. In addition, although the propagation delay is constant, the effectiveness of the hysteresis compensator depends on the resonant frequency and the load. Frequency is not an issue due to the fixed-frequency nature of the application, but effects of load changes deserve attention. Given that the delay depends on the current amplitude, the delay compensation circuit operates properly over a limited range of loads. In this sense, it must be noted that a heavier load results in a higher input current, which for the same hysteresis level V_{th} corresponds to a larger compensation, which results in

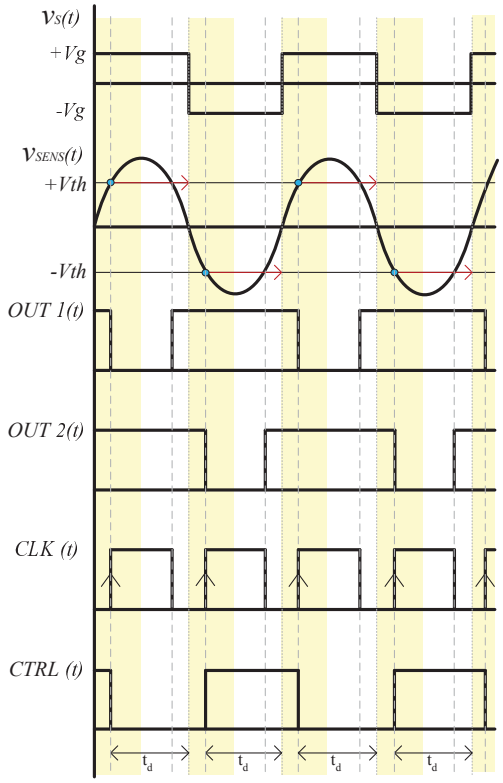

(a) with NAND gate.

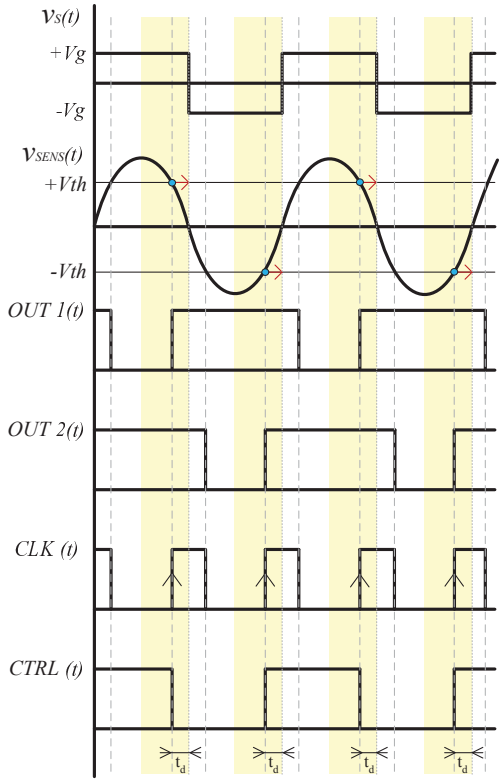

(b) with AND gate.

Figure 4. Hysteresis-based compensation waveforms

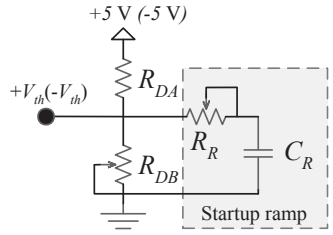

Figure 5. Lowpass filter of the hysteresis threshold enables self-oscillating start-up.

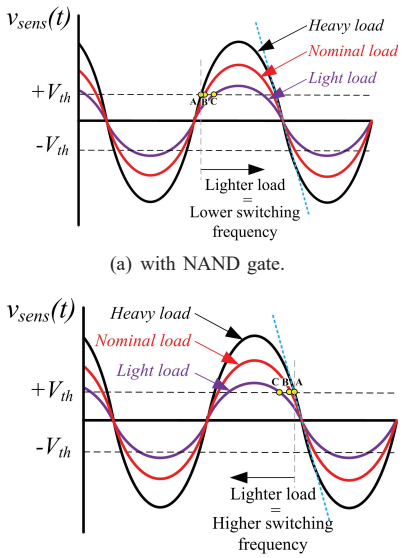

(a) with NAND gate.

(b) with AND gate.

Figure 6. Effect of load variation over the hysteresis applied. Circles: switching instants for different loads.

a higher switching frequency. In the present case, if the maximum load (R = 57 Ω) is associated with the maximum switching frequency f_{sw} = 6.93 MHz (6.78 + 0.15 Mhz), then the range of loads for which the allowed frequency range is accomplished equals [37, 57] Ω.

It is worth to point out that the range of valid operation depends on the power level of the design and also on the required compensation. The load range limits are established by the length of the zone surrounding the hysteresis level, which depends on the slope of the approximately sinusoidal input current as illustrated in Fig. 6. In the figure, it can be seen that for those levels in which the slope of the current can be considered linear, changes of current amplitude do not cause large changes in the switching frequency. Thus, the effects of this limitation may be potentially mitigated if the required delay values correspond to the area right before of after the zero crossings, where the influence of the current amplitude is minimal.

Regarding soft-switching, the hysteresis-based compensation network facilitates the accomplishment of ZVS if less than half semi-cycle is compensated (i.e., if the AND gate is used). Opposite to the behavior described above, lighter loads correspond, in this case, to higher switching frequencies,

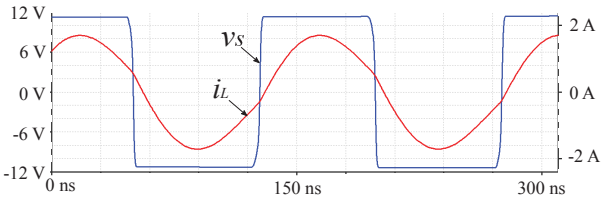

Figure 7. Output signal generated by simulation.

Table II. SUMMARY OF COMPONENTS IN THE EXPERIMENTAL PROTOTYPE

Component	Code or Value
L (Exp.)	300 nF
C (Exp.)	1.2 nF (C0G)
V_g	12 V
C_{in}	22.1 μF
Differential Amplifier	THS4151
eGaN FET (S_i)	EPC8004
Driver	LM5113
R_{SENS}	0.3 Ω
R_A,R_X	402 Ω
R_B,R_Y	2010 Ω
R_1,R_2,R_3,R_4	100 kΩ
R_{DA}	4 kΩ
R_{DB},R_R	100 kΩ
C_R	250 pF
NAND gate	NC7S08
JK monostable	SN74F109DR
Comparator	LT1116
Diodes (Rect.)	PMEG10020ELRX
L_f (Rect.)	1 μH
C_f (Rect.)	0.47 μF
R, R_L	57 Ω

allowing the circuit to resonate closer to the inductive zone of the input impedance, and facilitating the discharge of the parasitic capacitances in the switches. The differences between the AND and the NAND gate circuits can be more intuitively identified in Fig. 6.

C. Simulation Results

This subsection presents LTSpice simulations of the resonant converter with the designed hysteresis compensation network, in order to illustrate the operation of the circuit under the desired specifications. V_{th} has been adjusted in the simulation to compensate the delay and a startup ramp of 2 μs has been established for enabling auto-startup. Fig. 7 shows the steady-state waveforms of the input current, the input voltage and the hysteresis levels, confirming that the switching frequency with the selected delay compensation network is 6.78 MHz.

IV. EXPERIMENTAL RESULTS

An experimental prototype of the resonant converter with the proposed hysteresis compensation network has been built, following the specifications reported above. Resonant inductance and capacitance values have been modified to 300 nH and 1.2 nF, respectively, in order to account for the parasitic inductance of the circuit. Fig. 8 shows the schematic of the inverter and the inverter+rectifier configurations. As depicted, the inverter+rectifier configuration is obtained when the load is substituted by a full-wave rectifier and an LC filter. In both cases V_{th} is adjusted by an external voltage divider. Table II summarizes the components employed in the prototype, while Fig. 9 shows its picture.

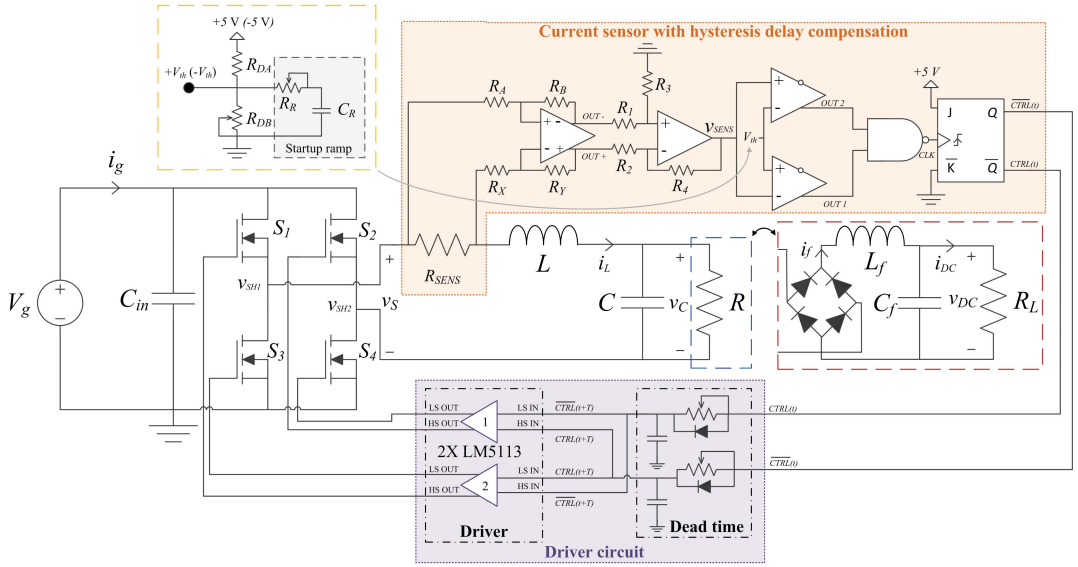

Figure 8. Schematic of the circuit for inverter and inverter+rectifier configurations.

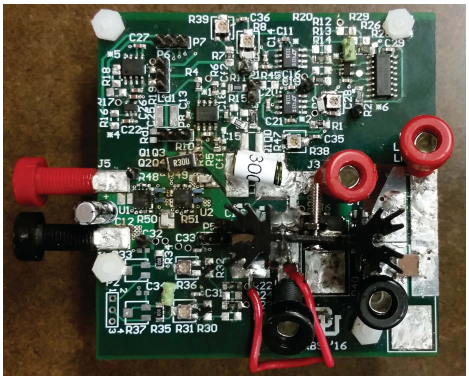

Figure 9. Photograph of the experimental prototype.

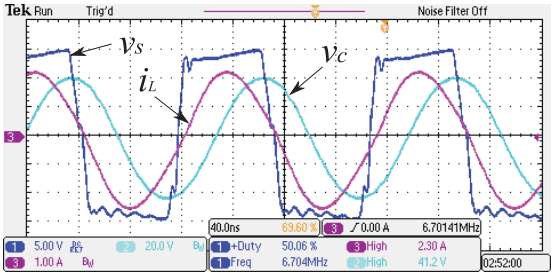

Figure 10. Input voltage, input current and capacitor voltage waveforms under nominal conditions.

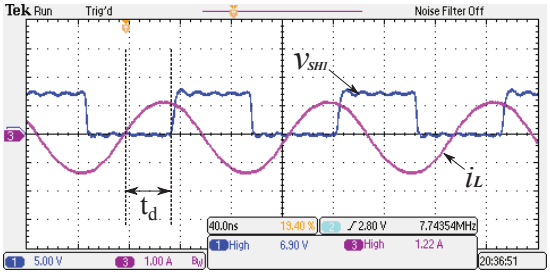

Figure 11. Positive input voltage and input current waveforms without delay compensation.

A. Inverter Configuration

Fig. 10 illustrates the experimental behavior of the circuit in steady-state self-oscillating operation, with the proposed delay compensation. The converter is able to startup and self-oscillate by simply applying power to the input port. The self-oscillating pattern generates a 12 V square-wave at the input of the resonant tank, which oscillates at a frequency of 6.78 MHz thanks to the delay compensator. At this frequency, an output average power delivery of 16 W for a load $R = 57\ \Omega$ is obtained, with an overall efficiency of 98 %. For comparison, Fig. 11 shows the operation of the converter with no delay compensation, clarifying the phase-shift between the input current and the input voltage.

The converter operates near ZVS at the nominal switching frequency. In Fig. 10, it can be seen that the square wave exhibits ringing at the end of the negative cycle, which denotes that ZVS is not fully achieved. An additional test, depicted in Fig. 12, shows that ZVS can be achieved if a slightly higher switching frequency, within tolerance limits of the Airfuel standard, is imposed (6.85 MHz). It should be noted that the prototype does not include a WPT inductor, and so the prototype is not capable of demonstrating wireless power transfer. Nonetheless, power stage characteristics are fully compliant with the AirFuel Alliance class 3 WPT standard.

B. Inverter+Rectifier Configuration

In addition, the applicability of this circuit as a small form factor wired battery charger is validated under its inverter+rectifier configuration. A switching frequency of 6.78 MHz is obtained for an output average power of 7 W with

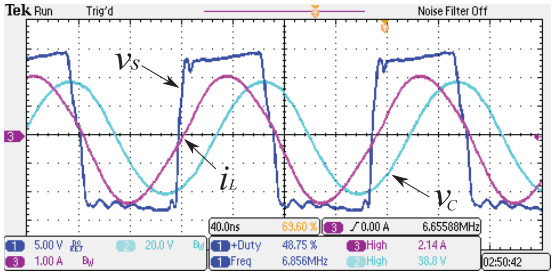

Figure 12. Input voltage, input current and capacitor voltage waveforms for a switching frequency of 6.85 MHz

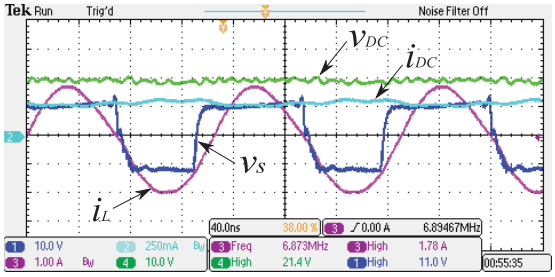

Figure 13. Input/output current and voltage waveforms in the inverter+rectifier configuration.

a load $R_L = 57\ \Omega$, as depicted in Fig. 13. The results comply with the requirements established by class 3 receiver of AirFuel Alliance standard. The power efficiency in this configuration is 83 %. The output power is significantly reduced with respect to the inverter configuration mainly due to the losses introduced by the diode bridge.

V. Conclusions

This paper proposes a self-oscillating resonant converter configuration for wireless power transfer applications according to the AirFuel Alliance standard. The proposed converter meets the main specifications of the standard, which for a class 3 transmitter include a switching frequency of 6.78 MHz and an output power of 16 W for a 57 Ω load. The main advantages of the proposed approach are the ability to auto-start and self oscillate while maintaining ZVS operation, and the relative simplicity of the circuit implementation.

The main challenges of the self-oscillating approach include the need for a delay-compensation network, accounting for the propagation delays of the driving circuit, in order to switch at the desired frequency. A hysteresis-based compensation method with soft startup has been introduced to address this challenge. The method is particularly well suited for fixed-frequency WPT applications.

The startup and operation of the proposed self-oscillating converter at 6.78 MHz and 16 W have been verified with an experimental prototype inverter using GaN devices, showing an efficiency of 98 %.

References

[1] F. Carobolante, "Wireless power transfer: Overcoming the technological hurdles," in *2013 Applied Power Electronics Conference (APEC)*, 2013.

[2] L. Chung, "Wireless power transfer technology," August 2015. [Online]. Available: http://www.eet-cn.com/STATIC/PDF/201509MAPS.pdf

[3] Alliance for Wireless Power, "A4WP Wireless Power Transfer System Baseline System Specifications (BSS)," November 2013.

[4] R. Tseng, B. von Novak, S. Shevde, and K. A. Grajski, "Introduction to the alliance for wireless power loosely-coupled wireless power transfer system specification version 1.0," in *Wireless Power Transfer (WPT), 2013 IEEE*, May 2013, pp. 79–83.

[5] H. G. Park, J. H. Jang, H. J. Kim, Y. J. Park, S. Oh, Y. Pu, K. C. Hwang, Y. Yang, and K. Y. Lee, "A design of a wireless power receiving unit with a high-efficiency 6.78-MHz active rectifier using shared DLLs for magnetic-resonant A4 WP applications," *IEEE Transactions on Power Electronics*, vol. 31, no. 6, pp. 4484–4498, June 2016.

[6] X. Lu, P. Wang, D. Niyato, D. I. Kim, and Z. Han, "Wireless charging technologies: Fundamentals, standards, and network applications," *IEEE Comm. Surveys Tutorials*, vol. 18, no. 2, pp. 1413–1452, 2016.

[7] M. A. de Rooij, "The ZVS voltage-mode class-D amplifier, an eGaN FET-enabled topology for highly resonant wireless energy transfer," in *IEEE Applied Power Electronics Conf. and Expo. (APEC)*, March 2015, pp. 1608–1613.

[8] E. P. C. Corporation, "Demonstration System EPC9111 Quick Start Guide: 6.78 MHz, ZVS Class-D Wireless Power System using EPC2014," 2015.

[9] M. d. Rooij, "Performance comparison for A4WP Class-3 Wireless Power Compliance between eGaN FET and MOSFET in a ZVS Class D Amplifier," in *PCIM Europe 2015; International Exhibition and Conference for Power Electronics, Intelligent Motion, Renewable Energy and Energy Management; Proceedings of*, May 2015, pp. 1–8.

[10] P. S. Riehl, A. Satyamoorthy, H. Akram, Y. C. Yen, J. C. Yang, B. Juan, C. M. Lee, F. C. Lin, V. Muratov, W. Plumb, and P. F. Tustin, "Wireless power systems for mobile devices supporting inductive and resonant operating modes," *IEEE Transactions on Microwave Theory and Techniques*, vol. 63, no. 3, pp. 780–790, March 2015.

[11] K. G. Moh, F. Neri, S. Moon, P. Yeon, J. Yu, Y. Cheon, Y. s. Roh, M. Ko, and B. H. Park, "A fully integrated 6W wireless power receiver operating at 6.78MHz with magnetic resonance coupling," in *2015 IEEE International Solid-State Circuits Conference - (ISSCC) Digest of Technical Papers*, Feb 2015, pp. 1–3.

[12] R. Bonache-Samaniego, C. Olalla, L. Martinez-Salamero, and H. Valderrama-Blavi, "Design of self-oscillating resonant converters based on a variable structure systems approach," *IET Power Electronics*, vol. 9, no. 1, pp. 111–119, 2016.

[13] R. Bonache-Samaniego, C. Olalla, and L. Martinez-Salamero, "Dynamic modeling and control of self-oscillating parallel resonant converters based on a variable structure systems approach," *IEEE Transactions on Power Electronics*, vol. 32, no. 2, pp. 1469–1480, 2017.

[14] J. Lautner and B. Piepenbreier, "Impact of current measurement on switching characterization of GaN transistors," in *IEEE Workshop on Wide Bandgap Power Devices and Appl. (WiPDA),*, Oct 2014, pp. 98–102.

[15] Y. Ye, D. Liang, J. Du, M. Tang, and X. Liu, "Design and optimization of high frequency current transformer," in *Int. Conf. on Electrical Machines and Systems (ICEMS)*, Oct 2014, pp. 963–966.

[16] L. Xu, Q. Chen, X. Ren, S. Ping, and S. C. Wong, "Self-oscillating contactless resonant converter with power transfer and current sensing integrated transformer," in *2015 IEEE Energy Conversion Congress and Exposition (ECCE)*, Sept 2015, pp. 4539–4543.

[17] F. Costa, E. Laboure, F. Forest, and C. Gautier, "Wide bandwidth, large AC current probe for power electronics and EMI measurements," *IEEE Transactions on Industrial Electronics*, vol. 44, no. 4, pp. 502–511, 1997.

[18] C. H. Chia, P. S. Lei, and R. C. H. Chang, "A high-speed converter with light-load improvement circuit and transient detector," in *IEEE International Symp. on Circuits and Systems*, May 2012, pp. 456–459.

[19] H. Mao, "High efficiency high frequency resonant power conversion," August 2014, US Patent App. 14/177,049.

[20] H. Li and S. Munk-Nielsen, "Challenges in switching SiC MOSFET without ringing," in *International Exhibition and Conference for Power Electronics, Intelligent Motion, Renewable Energy and Energy Management (PCIM)*, May 2014, pp. 1–6.